A dynamic and thermodynamic analysis of the 11 December 2017 tornadic supercell in the Highveld of South Africa

Lesetja E. Lekoloane[1,2], Mary-Jane M. Bopape[1], Gift Rambuwani[1], Stephanie Landman[1], Puseletso Mofokeng[1,3], Morne Gijben[1], and Ngwako Mohale[1]

[1]South African Weather Service, Pretoria, 0001, South Africa
[2]Global Change Institute, University of the Witwatersrand, Johannesburg, 2050, South Africa
[3]School of Geography, Archaeology and Environmental Studies, University of the Witwatersrand, Johannesburg, 2050, South Africa

Correspondence: Lesetja Lekoloane (lesetja.lekoloane@weathersa.co.za)

Abstract. On 11 December 2017, a tornadic supercell initiated and tracked through the northern Highveld region of South Africa for 7 hours. A tornado from this supercell led to extensive damage to infrastructure and caused injury and displacement of over 1000 people in Vaal Marina, a town located in the extreme south of the Gauteng Province. In this study we conducted an analysis in order to understand the conditions that led to the severity of this supercell, including the

5   formation of a tornado. The dynamics and thermodynamics of two configurations of the Unified Model (UM) were also analysed to see how they performed in predicting this tornadic supercell. It was found that this supercell initiated as part of a cluster of multicellular thunderstorms over a dryline, with three ingredients being important in strengthening and maintaining it for 7 hours: significant surface to mid-level vertical shear, an abundance of low-level warm moisture influx from the tropics and Mozambique Channel, and the relatively dry mid-levels. It was also found that the 4.4 km grid spacing model

10   (SA4.4) performed better than that of 1.5 km grid spacing (SA1.5). SA1.5 underestimated mid-level vorticity due to a significant underestimation in low-level warm moisture advection and convergence. SA4.4 captured the supercell but underestimated its severity due to an underestimation in mid-level vorticity found to be one order of magnitude smaller than that of a typical mesocyclone. This was a result of underestimation in surface to mid-level wind shear and low-level horizontal mass and moisture flux convergence. Future investigations will involve experimental research over the Highveld

15   region of South Africa to understand mesoscale and local dynamics processes responsible for tornadogenesis in some severe storms. Such a study, to the best of our knowledge, has never been conducted.

1 Introduction

Human survival and development have long been directly and indirectly dependant on weather and climate (Nuttall, 1998; IPCC, 2014). In their different spatial and temporal scales and reach, extreme weather events can result in prolonged

20   negative socio-economic impacts and affect different facets of the society including ecosystems (Meehl et al., 2000). Examples of these extremes include enormous and powerful synoptic tropical systems such as Tropical Cyclones Eline in

2000 (Reason and Keibel, 2004) and Idai in 2019 (WMO, 2019) which affected millions of people in southern African mainland; or the unusually extended tornado outbreak across the central and eastern United States during May 2003 which resulted in about $829 million of property damage (Hamill et al., 2005). Growing evidence suggests that more of these

25   extreme events are becoming a commonality in some parts of the world, and can be expected to increase in intensity and frequency due to climate change (e.g. Handmer et al., 2012; Melillo et al., 2014; EASAC, 2018).

There is no region on Earth immune to extreme or severe weather events, but communities most critically affected are especially those from developing countries (Mirza, 2003). For example, many developing countries' economies and livelihoods are highly depended on primary sectors of the economy (UN, 2018a) such as agriculture and fishing of which

30   negative effects have already been experienced due to an increase in high impact weather events (Adger et al., 2003; Awojobi and Tetteh, 2017). Therefore, an understanding of these high impact weather events, and being able to predict them precisely, is of importance for sustainable development as well as mitigation and adaptation strategies.

One of the regions identified as highly vulnerable to climate change and its effects is sub-Saharan Africa (Boko et al., 2007). Most countries in this region of the world are lacking behind in the development scale and have many stressors

35   including high impact weather events (UN, 2018b). Although no single weather event can be confidently attributed to climate change, an increasing number of studies are documenting a positive trend of severe weather events in southern Africa (Davis-Reddy and Vincent, 2017; Kruger and Nxumalo, 2017). These include an increase in the frequency of extreme rainfall events associated with land-falling tropical cyclones and severe thunderstorms, particularly in the eastern parts of southern Africa and south of South Africa (Malherbe et al., 2013; Engelbrecht et al., 2013).

40   A climatological analysis over South Africa indicates an increase in extreme rainfall events, especially during spring and summer months (Engelbrecht et al., 2013; DEA, 2016) mostly in the form of convective precipitation (Tyson and Preston-Whyte, 2000; Hart et al., 2013). The eastern parts of South Africa are dominated by thunderstorms during summer months which often result in fatalities, serious injuries, and extensive damage to infrastructure including crops and livestock (Gijben, 2012; NDMC, 2018).

45   Thunderstorms are primarily classified either as single cell, multicell or supercell – the latter two types could become very severe and destructive, with supercell thunderstorms notoriously known for producing spectacular tornadoes (Houze, 1993). It should be noted that some severe forms of multicell thunderstorms can also produce tornadoes, and that not all supercell thunderstorms produce tornadoes (Markowski and Richardson, 2009). Tornadoes are common around the world, but the most severe are often reported in the United States of America (e.g. Hamill et al., 2005).

50   South Africa experiences a significant number of severe thunderstorms annually, especially during summer months over the Highveld (Gijben, 2012). A few of these intensify to severe supercell type and often results in strong damaging winds, large hail and tornadoes (Rae, 2014; Glickman, 2000). Tornadoes can occur anywhere in South Africa, but they are frequently reported in the Highveld regions of Gauteng, north-eastern Free State, western Mpumalanga, and south-central KwaZulu Natal (Goliger and Retief, 2007).

55   Research has shown that the possible two main important factors for the initiation of tornadoes in thunderstorms are: large amounts of low-level water vapour and the presence of boundary layer vertical wind shear (Markowski and Richardson, 2009). For this reason, near-surface large vertical vorticity is a prerequisite for tornadogenesis. There are two possible ways in which this near-surface vertical vorticity could arise: either through advection of vorticity from aloft or through tilting of environmental horizontal vorticity in supercell thunderstorms (Markowski and Richardson, 2009).

60   A recent study by Dahl (2017) has however shown that the tilting of horizontal vorticity alone is not enough to produce a rotating updraft in supercells. For the tilting of horizontal vorticity, a downdraft is needed possibly at the rear-flank of the storm to pair the updraft in the inflow side of the storm (Davies-Jones et al., 2001). However, this downdraft is not necessary if near-surface vertical vorticity pre-existed before the storm genesis, in which case near surface convergence alone is enough for tornadogenesis (Markowski and Richardson, 2009). Davies-Jones (2015) has summarised tornadogenesis in supercells as occurring in three stages: the formation of mesocyclone in the mid-level, rotation at the ground, and tornado formation or failure.

      On 11 December 2017, a supercell thunderstorm associated with large hail, strong damaging winds and a tornado tracked through Vaal Marina, a town in the extreme south of the Gauteng Province of South Africa. The tornadic supercell led to trees being uprooted, destroyed commercial and residential properties, and left about 50 people injured, including several animals, and over 1100 informal settlement dwellers displaced (SAWS, 2018). The aim of this study is to perform an analysis of this supercell in order to understand the conditions that led to its severity including the formation of a tornado in Vaal Marina. The dynamics and thermodynamics of two configurations of a numerical weather prediction (NWP) model operationally run at the South African Weather Service (SAWS) are also analysed and evaluated to see how they performed in predicting this tornadic supercell.

2 Data and methods

2.1 Area of interest

The focus area of this study is in the northern parts of the Highveld region of South Africa, and covers Vaal Marina located in the extreme south of the Gauteng Province, and the storm track in the Free State and Mpumalanga provinces as shown in Fig. 1. The locations of SAWS radars used to track the storm of interest and weather stations where data were analysed for mesoscale circulations, in this study, are also shown on Fig. 1.
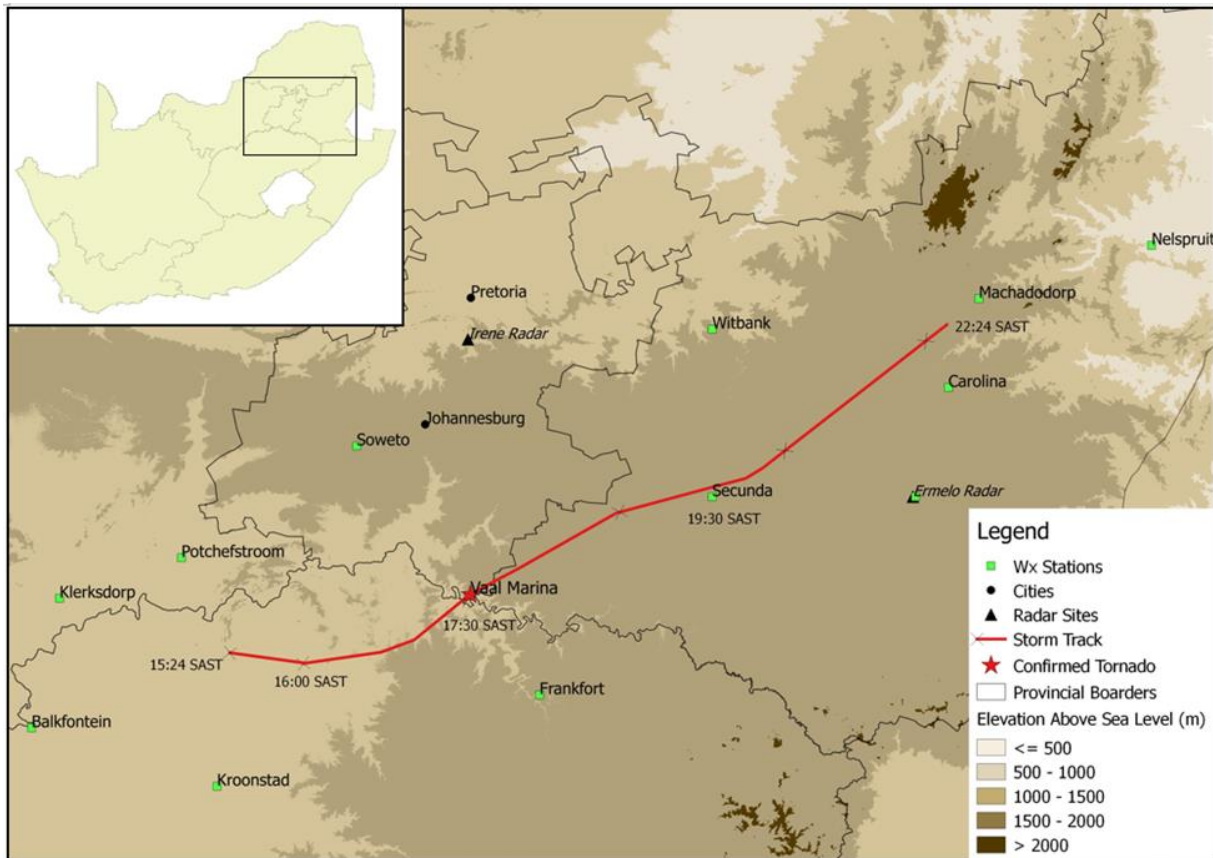
Figure 1: The map of South Africa highlighting northern parts of the Highveld (defined as enclosed by the 1500 m above sea level height). The supercell track is indicated with a red line and includes the location of the storm at local times during its 7-hour propagation. Weather stations (Wx Stations) where surface data were analysed for mesoscale circulations are also indicated including the location of the Vaal Marina tornado.

2.2 Datasets

2.2.1 The Unified Model

The primary model data analysed in this study are from the Unified Model (UM) (version 10.4). The UM is a seamless and deterministic numerical modelling system originally developed by the United Kingdom's Meteorological Office (UKMO) for weather prediction and climate studies (Davies et al., 2005). This model is operationally run four times a day on the SAWS CRAY XC-30 high performance computing system. Initial and boundary conditions from the Global Atmosphere (GA, Walters et al., 2017) are used as the driving data for the purpose of producing short-range operational weather forecasts of up to 3 days ahead.

The UM is run in two configurations of the regional and sub-regional domains with 70 vertical levels. The first configuration runs at a horizontal grid length of 4.4 km (this configuration is hereafter referred to as SA4.4) and covers the

domain from 0° S to 36° S and 5° E to 54° E. This setup essentially covers the Southern African Development Community (SADC) except the northern parts of Democratic Republic of Congo. The second configuration is centred over South Africa from 20° S to 36° S and 15° E to 34° E and is run at a horizontal grid length of 1.5 km (this configuration is hereafter

95 referred to as SA1.5). The model configurations analysed in this study were both operationally initialised and run at 00:00 UTC on 11 December 2017.

The dynamical core of the model configurations in this study uses a semi-implicit semi-Lagrangian formulation to solve the non-hydrostatic, fully-compressible deep-atmosphere equations of motion (Wood et al., 2014). On the other hand, physical parameterisations of sub-grid processes are split into slow processes (radiation and microphysics) and fast processes

100 (atmospheric boundary layer turbulence, cloud and surface coupling) which are treated and computed differently.

2.2.2 Radiosonde, station and radar data

To perform an analysis of the thunderstorm and its proximal environment during its lifecycle, surface weather station data and radar data are obtained from the SAWS weather station and radar networks. Surface observation data from a total of up to 228 automatic weather stations across South Africa, were regridded and used for synoptic analysis. Only a selected

105 number of stations proximally closer to the storm track in the Free State, Gauteng and Mpumalanga provinces were used for mesoanalysis (see Fig. 1). The surface stations data used contain temperature, dewpoint temperature, pressure, wind speed, wind direction, and rainfall.

To capture data from middle to lower levels of the storm, the Irene (25.87° S, 28.22° E) and Ermelo (26.53° S, 30.03° E) weather radars are used to track the storm throughout its cycle, from initiation to dissipation (see Fig. 1).

110 A 1200 UTC Irene weather office's Radiosonde sounding, on the day considered, is used as a proximity sounding of the atmospheric conditions at Vaal Marina. The Irene weather office is located about 110 km north of Vaal Marina and is therefore within the proximity sounding criteria for the location as defined by Craven and Brooks (2004).

2.2.3 Reanalysis data and synoptic analysis

A fifth generation European Centre for Medium-Range Weather Forecasts (ECMWF) reanalysis of the atmosphere (ERA5)

115 on single levels and pressure levels, hourly data are utilised to analyse synoptic meteorological conditions of the day. The ERA5 dataset is the state-of-the-art atmospheric reanalysis of the global climate with a horizontal grid length of 0.25°×0.25° and 137 vertical levels up to 1 Pa (Hersbach and Dee, 2016). Parameters analysed from this dataset include 10 m winds, mean sea level pressure, and geopotential heights at 850 -, 500, and 200 hPa levels.

2.2.4 Dynamic and thermodynamic analysis

120 In this study, both the 4.4 km and 1.5 km horizontal grid spacing of the model configurations are not high enough to reliably use only wind vectors as a determinant of organised mesoscale rotation. As an alternative, vorticity is used as a measure of rotation.

Vorticity is a curl of velocity and gives the measure of a fluid's infinitesimal rotation (Holton and Hakim, 2013). Ignoring the effects of friction, the Boussinesq approximation of the vorticity equation can be written as,

$$\frac{\partial \overline{\boldsymbol{\omega}}}{\partial t} = \nabla \times (\overline{\boldsymbol{V}} \times \overline{\boldsymbol{\omega}}) + \nabla \times (B\hat{k}) \tag{1}$$

Where $\overline{\boldsymbol{\omega}} = (\xi, \eta, \zeta)$ and $\overline{\boldsymbol{V}} = (u, v, w)$ respectively represents vorticity and velocity vectors in the horizontal (x-,y-axis) and vertical (z-axis), and B is the buoyancy.

It is not uncommon for thunderstorms to rotate, with supercell thunderstorms spectacularly distinguished by an even stronger and persistent vertically rotating updraft (Doswell and Burgess, 1998; Houze, 1993). Consequently, the current study utilises the vertical component of relative vorticity ζ as a diagnostic tool of rotation in the vertical axis. It can be derived from Eq. 1 to get,

$$\frac{\partial \zeta}{\partial t} = \hat{k} \cdot \nabla \times (\overline{\boldsymbol{V}} \times \overline{\boldsymbol{\omega}}) + \hat{k} \cdot \nabla \times (B\hat{k}) \tag{2}$$

It should be noted from Eq. 2 that $\hat{k} \cdot \nabla \times (B\hat{k}) = 0$. This implies that buoyancy is not directly responsible for the generation of vertical vorticity and therefore vertical rotation in thunderstorms. Further simplifying Eq. 2 gives,

$$\frac{\partial \zeta}{\partial t} = -\overline{\boldsymbol{V}} \cdot \nabla \zeta + \overline{\boldsymbol{\omega}}_H \cdot \nabla_H w + \zeta \frac{\partial w}{\partial z} \tag{3}$$

where the terms on the right-hand side of the equation respectively represents the advection, tilting and stretching terms.

In this study our dynamical definition of a mesocyclone follows that of Glickman (2000), which defines it as a cyclonically rotating vortex in a thunderstorm associated with vorticity on the order of $10^{-2}s^{-1}$ or greater. The horizontal scale of this vortex is normally somewhere between 2 to 10 km in a thunderstorm.

The presence of boundary layer water vapour concentration is one of the most important factors for tornadogenesis (Markowski and Richardson, 2009). As a result, to analyse the significance of low-level moisture in the event considered, the convergence of moisture flux is computed at 800 hPa level. Moisture flux convergence (MFC) is a useful diagnostic tool as it combines the effects of moisture advection and convergence and can be computed at any atmospheric pressure level (Banacos and Schultz, 2005).

To derive an equation for MFC, the conservation of water vapour is used and is further expanded and written in flux form using the continuity equation to get:

$$\frac{\partial q}{\partial t} + \nabla \cdot (q\overline{\boldsymbol{V}}_h) + \frac{\partial}{\partial p}(q\omega) = S = E - P \tag{4}$$

where q is the specific humidity and the second and third terms respectively represents horizontal and vertical moisture flux divergence. S represents the sources and sinks of the air parcel's water vapour evaporation rate (E) and precipitation rate

150 (P), assuming that all condensed water precipitates immediately. MFC is computed by taking the negative of the horizontal moisture flux divergence in Eq. 4, which gives,

$$MFC = -\nabla \cdot (q\bar{V}_h) = -\left(u\frac{\partial q}{\partial x} + v\frac{\partial q}{\partial y}\right) - q\left(\frac{\partial u}{\partial x} + \frac{\partial v}{\partial y}\right) \tag{5}$$

The terms on the right-hand side of Eq. 5 represents the advection of specific humidity (the advection term) and the product of specific humidity and horizontal mass convergence (the convergence term).

3 Results and discussion

155

Media reports indicated that on the late afternoon of 11 December 2017, a severe thunderstorm which resulted in extensive damage, tracked through the extreme south of the Gauteng Province of South Africa (Mitchley, 2017). Some eyewitnesses reported seeing a tornado close to Deneysville near the Vaal Dam, which later made its way to Vaal Marina and Mamello informal settlement (all these locations are hereafter collectively referred to as VAM) (Mashaba and ANA reporter, 2017).

160 Witnesses also reported strong, damaging winds and large hail (SABC, 2017). Visual impacts of the observed severe storm were also captured by some reports, and indicate uprooted trees, damaged houses and shacks, including damaged infrastructure such as overhead power lines (Storm Report SA, 2017). From these vast reports, it is clear that this was a high impact weather system, and therefore important to analyse – especially as climate change is expected to increase the frequency and intensity of high impact weather events which may disrupt social and economic progress.

3.1 Synoptic setting and meteorological conditions of 11 December 2017

165

On 11 December 2017, analysis indicates the presence of a ridging anticyclone which extended north of the south-eastern subcontinent and in the process of breaking-off from the parent Atlantic anticyclone to merge with the south Indian Ocean anticyclone located east of South Africa (Indicated by letter H over South-West Indian Ocean, SWIO; Fig. 2(d)). The Atlantic anticyclone began ridging behind a cold front which moved over south of the continent between 08 and 09

170 December and was located south-east of the continent on 10 December. The ridging anticyclone, which was situated in the south-eastern subcontinent on 10 December, led to an influx of warm and unstable low-level moisture from SWIO through the Mozambique Channel into the eastern and central provinces of South Africa: Mpumalanga, Limpopo, Gauteng, North West and Free State. The northward-extended, and now breaking, ridging anticyclone on 11 December was coupled with a deepened surface trough in the central interior of South Africa (Indicated by letter L over South Africa; Fig. 2(d), cf. Fig.

175 2(c)), resulting in moisture level increase in the eastern half of the country due to warm tropical inflow of unstable airmass.

Synoptic Analysis for 11 December 2017 12-UTC
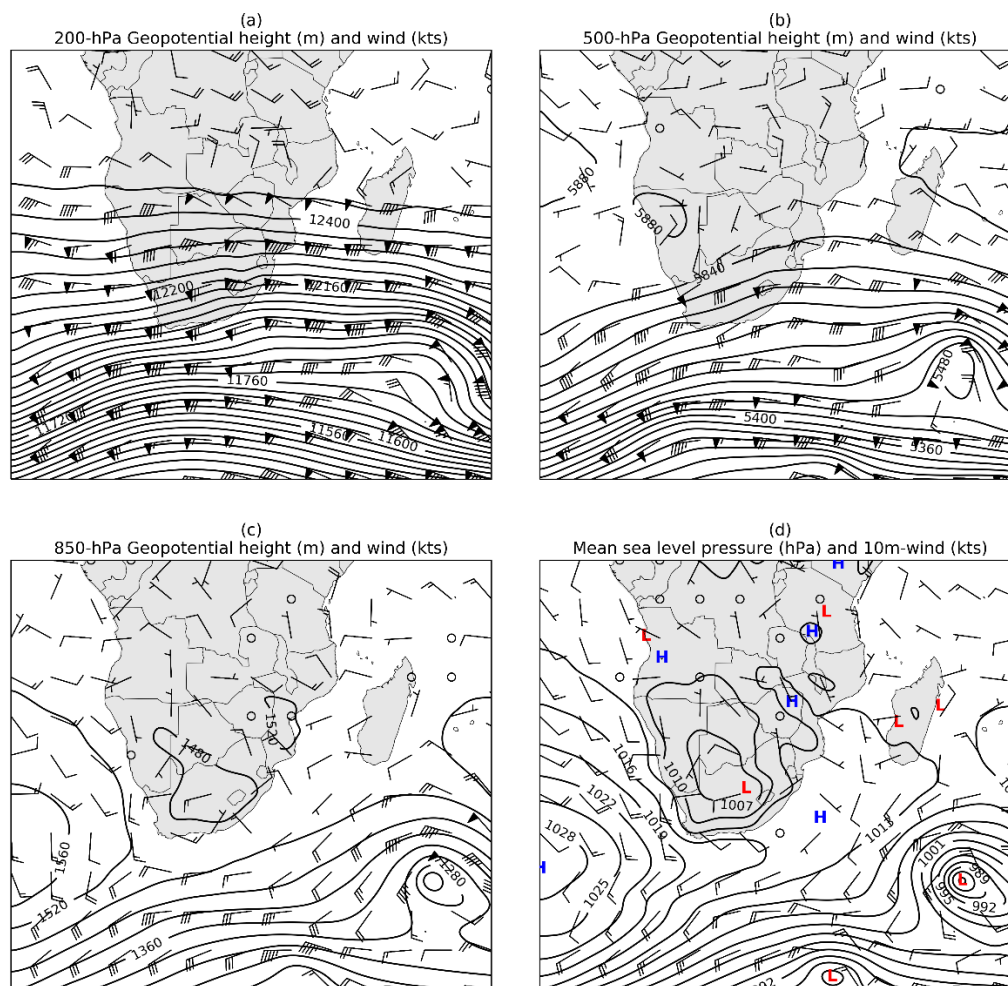
Figure 2: Synoptic chart analysis indicating mean sea-level pressure (in hPa) and 850-, 500- and 200 hPa Geopotential heights for 11 December 2017 at 1200 UTC over southern Africa and the surrounding oceans. Descriptions for each frame are contained in the body text.

The analysis also indicates the presence of a mid-tropospheric trough over the south-east of the continent and a ridge extending over Namibia and the western parts of South Africa (Fig. 2(b)). This mid-level circulation patterns resulted in mid-atmospheric south-westerly winds over the interior of South Africa, which enhanced convective instability over the central-east of the country as the dry mid-level air advects over the low-level warm and moist-air in the east. A weak upper-air trough was also present over South Africa (Fig. 2(a)).

These synoptic settings and conditions (as indicated in Fig. 2) resulted in the western-half of South Africa being hot and dry, while the eastern parts were cool and moist with low-level clouds present. The 12:00 UTC surface dew-point temperature analysis for 11 December 2017 conducted by operational forecasters at the SAWS, indicated the presence of a

dryline over the central Free State Province, which extended through the south-western areas of the North West Province and south-western parts of Botswana. The dryline separated the hot dry air in the west from the warm moist air in the east, and was moving eastwards after sunrise as differential heating allowed vertical mixing to entrain dry air from the west into the

190 moist boundary layer to the east of the dryline. This dryline was responsible for initiating several severe convective storms in the Free State Province, from which one intensified into a supercell thunderstorm that lasted for 7 hours and resulted in the observed VAM tornado.

3.2 Mesoanalysis

Surface station data along near thunderstorm track were used for mesoanalysis. Data analysis from radar and four weather
195 stations close to the location of the storm initiation (Potchefstroom, Soweto, Klerksdorp and Kroonstad) indicates that the storm of interest initiated after 13:00 UTC over a dryline. Fig. 3 and 4 indicates that along the dryline, there was a convergence of moist northerly winds and relatively dry westerly winds. Throughout the analysis period (from 10:00 to 22:00 UTC) Potchefstroom and Soweto recorded an advection of moist air from northerly winds, which respectively averaged 25 and 17 kts between 13:00 and 14:00 UTC (Fig. 3 and Fig. 4(a) and 4(b)). During the same analysis period,
200 stations at Klerksdorp and Kroonstad reported an advection of warm moist air from north-westerly winds which eventually became hot and dry and changed to westerly after a passage of the dryline (Fig. 3 and Fig. 4(c) and 4(d)). The average hot and relatively dry winds in those stations between 13:00 and 14:00 UTC was 33 kts, with Kroonstad respectively recording 43 and 33 kts.
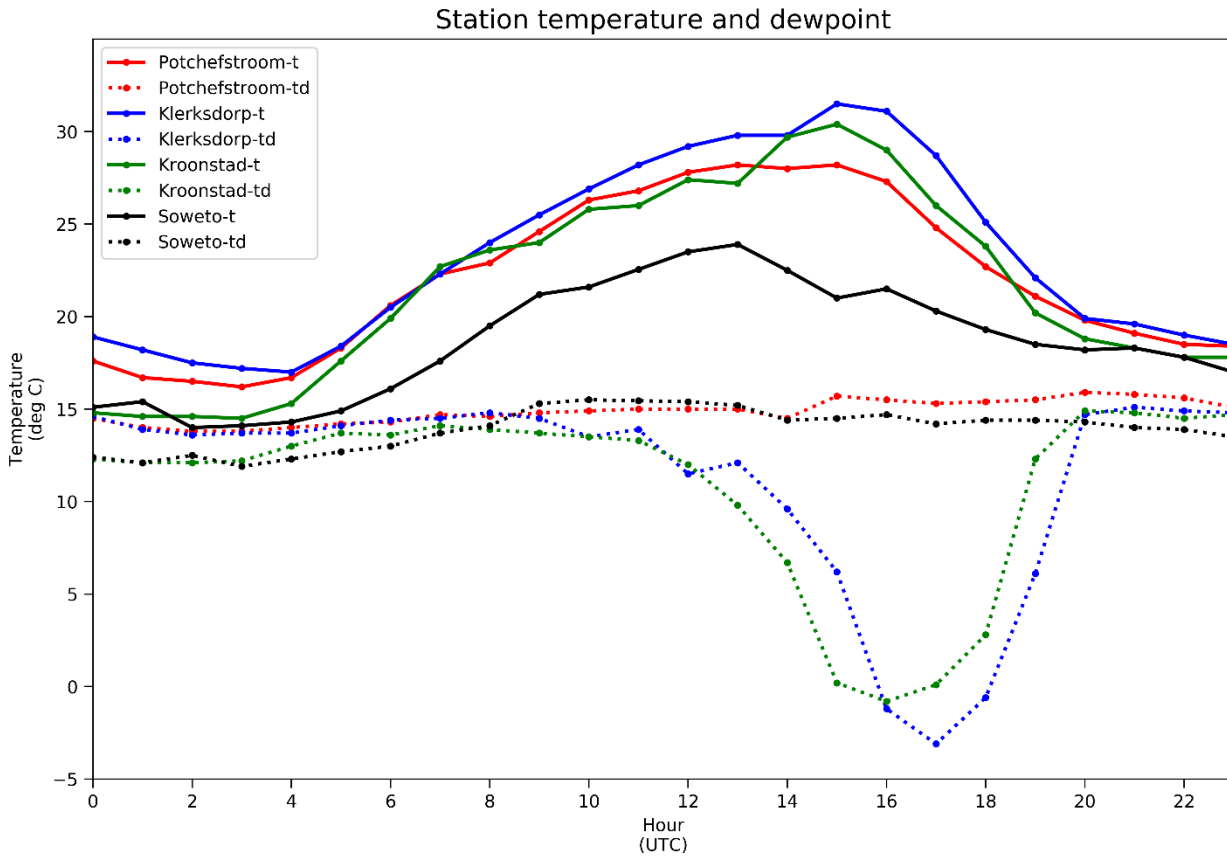
Figure 3: The graph is indicating changes in temperature and dewpoint temperature as reported by four weather stations located proximally closer to the location of the storm initiation between 00:00 UTC and 23:00 UTC on 11 December 2017.

205

After initiation, the storm initially propagated eastwards, then suddenly changed direction to north-east towards the Vaal Dam as it matured into a supercell thunderstorm through energy supply from a continual merger of several cells. As the supercell approached the Vaal Dam, it intensified further and was now associated with large hail and strong damaging winds, with the first sighting of a tornado near Deneysville (town in the north-western edge of the Vaal Dam). The now tornadic

210 supercell then moved across the Vaal Dam and reached Vaal Marina (town in the north-eastern edge of the Vaal Dam), in the extreme south of Gauteng Province. In Vaal Marina (and Mamello informal settlement), the supercell was still associated with large hail, strong damaging winds, and a tornado touchdown of about 1.5 km (1500 m) was confirmed from site visit (and by confirming this in situ data with radar and satellite data).
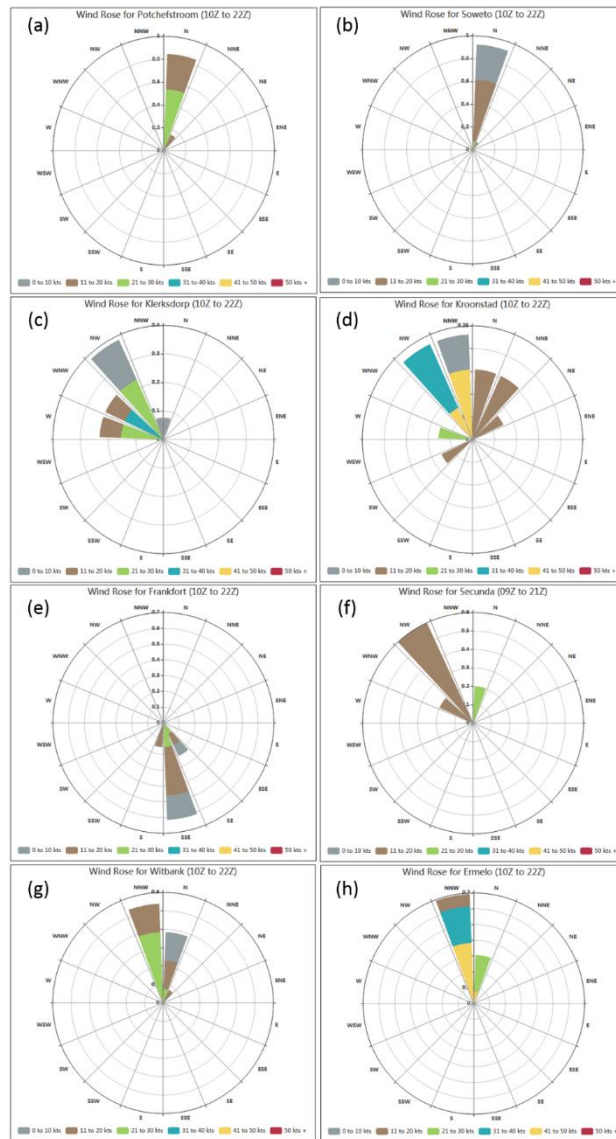
Figure 4: Wind rose diagrams of eight weather stations proximally closer to the storm track (as depicted in Fig. 1) between 10:00 and 22:00 UTC on 11 December 2017.

215

It might be significant to note that Frankfort station located a little over 50 km south-south-east of VAM (see Fig. 1) reported cool and moist southerly to south-easterly winds almost throughout the day (Fig. 4(e)) while stations north of VAM reported cool to warm and moist northerly to north-westerly winds. There is not enough surface data in the vicinity and south of VAM to know whether Frankfort wind speeds and directions generally represent mesoscale circulation at locations south

220   and proximally closer to VAM since it is the only station available around that area. If it does represent mesoscale

circulation south of VAM, then it is more likely that there was convergence of cool and moist air close to VAM before tornadogenesis occurred between Deneysville and Vaal Marina.

The 12:00 UTC Irene upper-air sounding (Fig. 5) captured north-north-easterly cool and moist surface winds of 10 kts which back with height (turns counter-clockwise with height, comparative to veering in the Northern Hemisphere) to west-
south-westerly at 500 hPa to become 25 kts. The upper-air sounding in Fig. 5 confirms winds captured by the synoptic analysis in Fig. 2 close to the sounding's vicinity. This indicates significant directional shearing between the surface and the mid-troposphere, while the speed shearing was respectively weak (15 kts at 500 hPa) to moderate (40 kts at 300 hPa). The sounding also indicates a 35 kts lower mid-level jet and an upper-level west-north-westerly jet of 65 kts, which also confirm the synoptic analysis in Fig. 2. The lower levels were moist with an average relative humidity of 91% between the surface
and 625 hPa, while the mid-levels were dry with relative humidity averaging 26% between 573 hPa and 400 hPa. Therefore, the availability of low-level moisture, dry mid-levels, and vertical wind shearing provided favourable conditions for the possibility of dynamically and thermodynamically induced organised severe thunderstorms (including supercell type) developing in the vicinity.
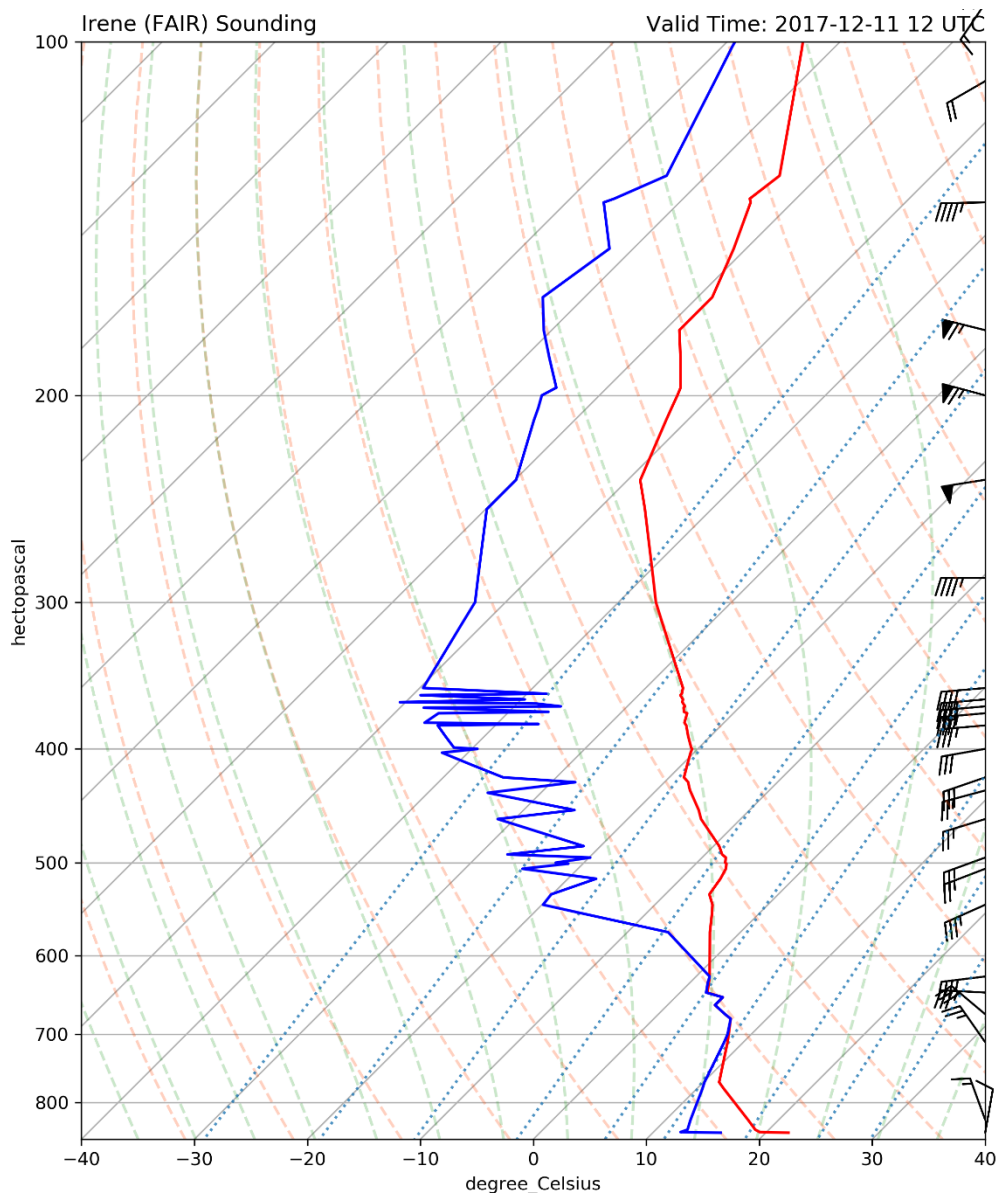
Figure 5: Irene upper-air sounding at 1200 UTC on 11 December 2017. This is used to proximate atmospheric conditions over VAM.

235

    A hook echo, which confirms that this severe thunderstorm was a supercell, can clearly be seen from the low-levels of the storm between 15:16 UTC and 15:34 UTC as observed by the first sweep of the Irene radar (at an elevation angle of 0.5°) (Fig. 6). Figure 6(a) indicates a hook echo west of the Vaal Dam at 15:16 UTC which was associated with local strong cyclonically rotating winds as indicated by the radial velocity inbound-outbound maxima in Fig. 6(b) (this could explain the

240   tornado observed near Deneysville). A hook echo was also observed 12 minutes later at 15:28 UTC over Mamello, an

informal settlement located in the eastern outskirts of Vaal Marina (Fig. 6(e)). Figure 6(f) indicates that this hook echo over Mamello was also associated with local strong circulating winds. This analysis indicates that it is most likely that the tornado that was reported to have devastated VAM touched down multiple times between 15:15 and 15:30 UTC (17:15 and 17:30 local time); but could also have been on the ground during this entire period or for a period longer than the mesocyclone that was captured by the radar.

245
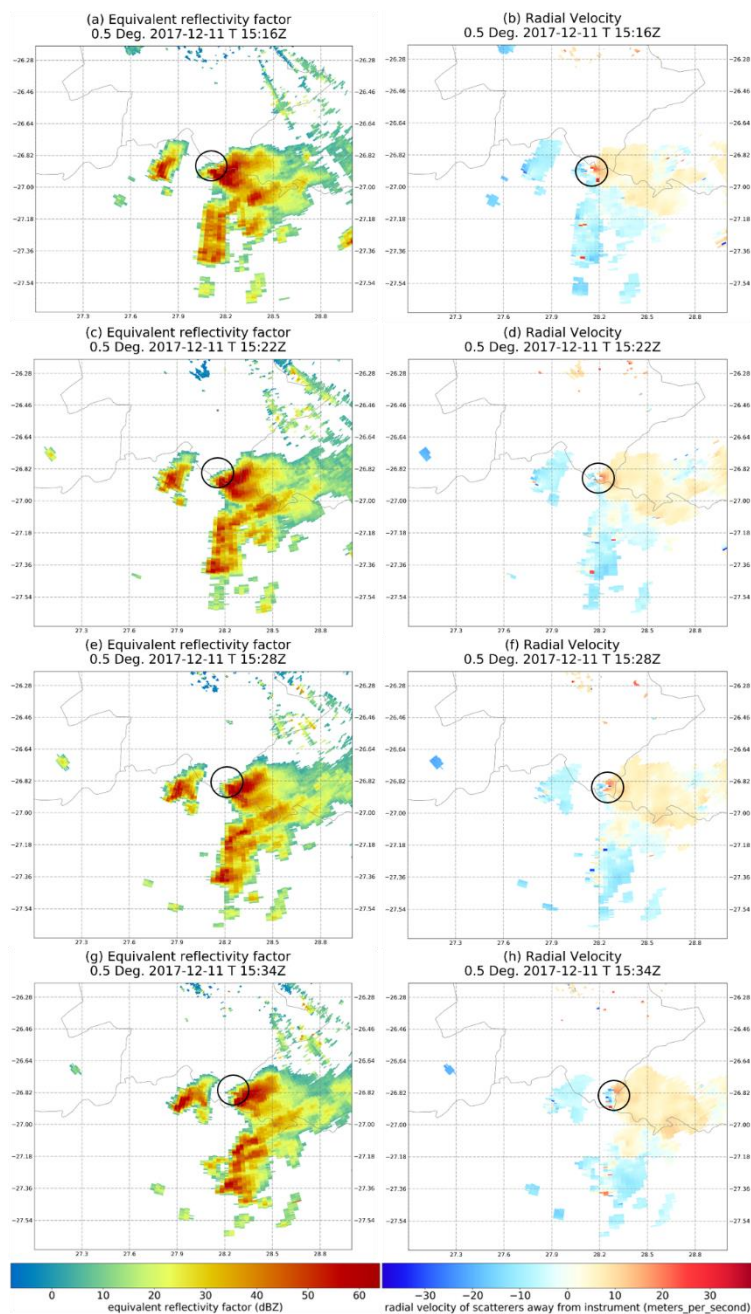
Figure 6: Irene radar equivalent reflectivity factor (dBZ) and radial velocity of scatterers (m/s) of the supercell thunderstorm as plotted using Python ARM Radar Toolkit (Py-ART) (Helmus and Collis, 2016). The left-hand column indicates low-level reflectivity as captured by the first radar sweep at an elevation angle of 0.5° for every 6 minutes, between 15:16 UTC and 15:34 UTC. The right-hand column radar scans have similar properties as the left-hand column radar scans but for the radial velocity of scatterers.

After passing through the VAM area, the supercell continued in the north-easterly direction, weakening and strengthening throughout, before dissipating just before reaching Machadodorp in Mpumalanga Province. Throughout near storm track (except for Frankfort), surface winds were variable between northerly and north-westerly (Fig. 4). The supercell dissipated on approach to Machadodorp where winds were variable between north-easterly to easterly between 19:00 and 20:00 UTC (21:00 and 22:00 local time) and averaged 8 kts.

3.3 Unified Model analysis

SA4.4 predicted a precipitating storm propagating north of VAM between 15:00 and 16:00 UTC (Fig. 7(a)). The timing of this precipitating storm as predicted by SA4.4 was correct; however, the location was slightly north of the actual observation (cf. Fig. 6). On the other hand, SA1.5 failed to predict any precipitation close to VAM between 15:00 and 16:00 UTC or anytime during the analysis period (between 12:00 to 24:00 UTC) (Fig. 7(b)).
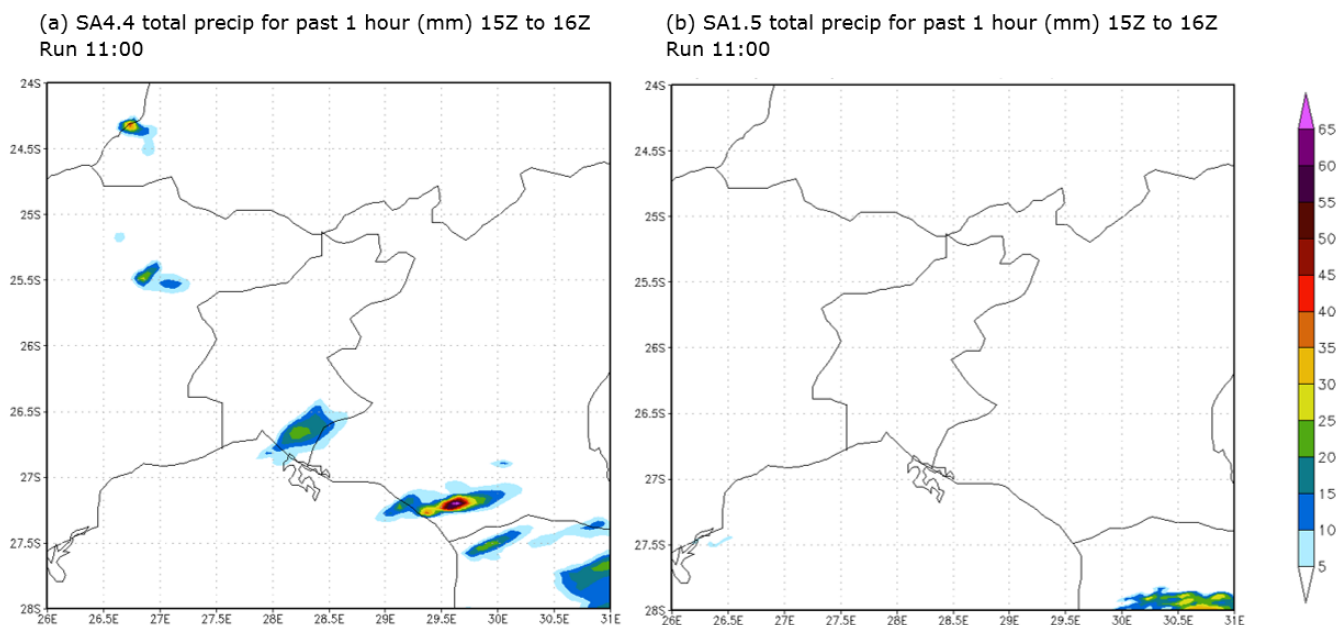
Figure 7: Total precipitation for the past 1 hour between 1500 and 1600 UTC (in mm) as predicted by (a) SA4.4 and (b) SA1.5. The shaded scale is in the interval of 5 mm.

An analysis of the 10 m wind directions in SA4.4 and SA1.5 generally agrees with observed surface northerly to north-westerly wind directions close to VAM, however the wind speeds are underestimated in both models (Fig. 8). Figures 8(b) and 8(d) show that SA4.4 and SA1.5 predicted almost similar wind speeds at 15:00 UTC, which are underestimated compared to observations (Fig. 8(a)). A sample of three stations along the storm track taken proximally closer to the location of initiation, propagation and dissipation stages of the storm (Klerksdorp, Witbank and Machadodorp) indicate that SA4.4

265   and SA1.5 especially underestimated the wind speeds during the initiation stage of the storm (Fig. 8(c)). Both models also
generally indicate westerly and south-westerly 500 hPa winds at 15:00 UTC over VAM (Fig. 9(a) and 9(b)). Considering
surface winds, both models indicate the presence of vertical shear between the surface and the mid-levels, however the speed
shearing is possibly underestimated especially during the initiation phase of the storm.
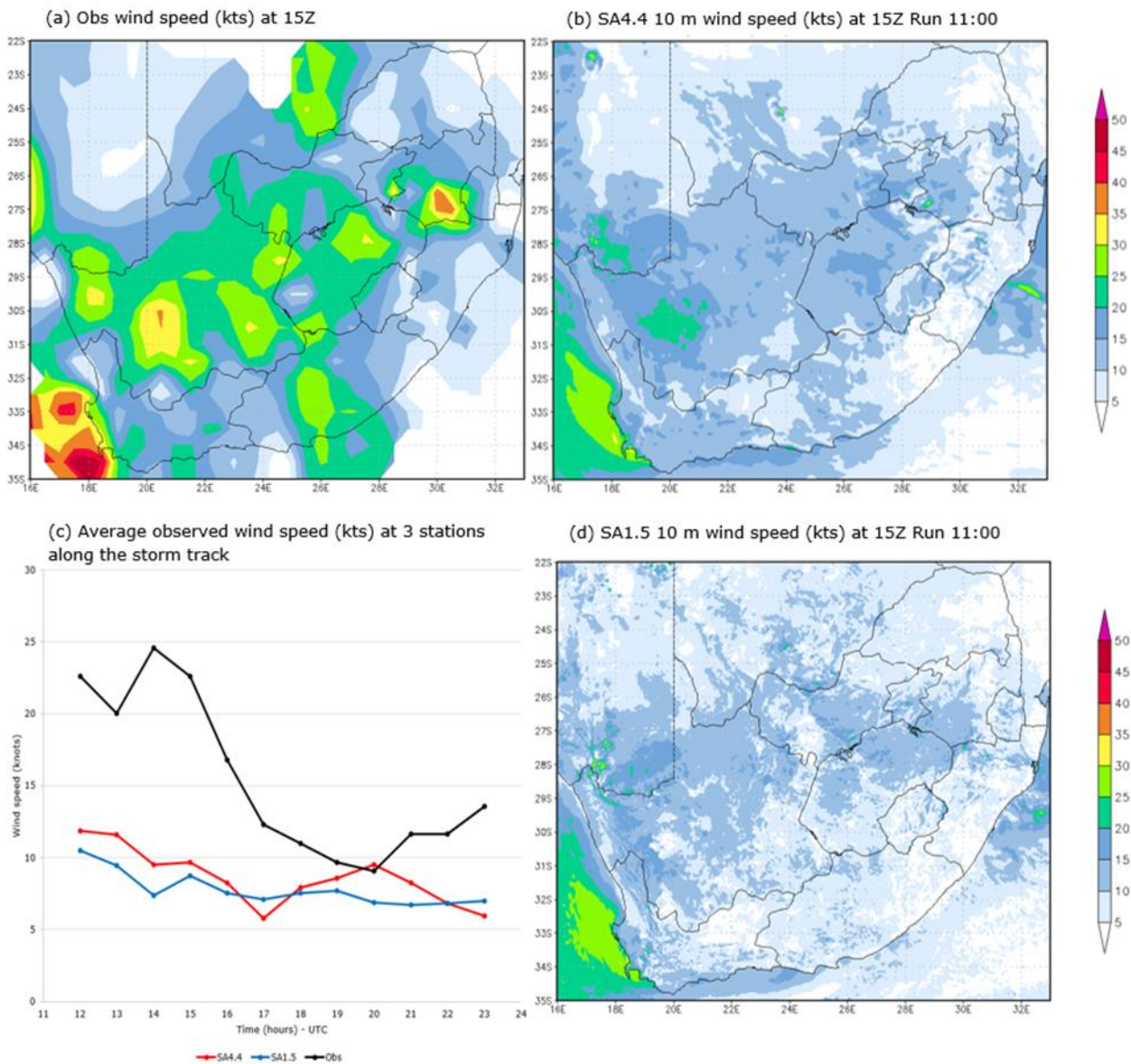
Figure 8: A comparison of (a) Regridded observed surface wind speed from weather stations across South Africa at 15:00 UTC with 10 m
predicted winds by (b) SA4.4 and (d) SA1.5. Figure (c) indicates a comparison of average wind speeds from three stations along the storm

track (Obs) compared to SA4.4 and SA1.5 data for those stations between 12:00 UTC and 23:00 UTC. All the wind magnitudes are given in knots at an interval of 5 knots.

270

SA1.5 failed to predict any precipitation close to VAM (Fig. 7(b)). This can be attributed to a failure in predicting any significant low-level convergence of moisture fluxes anywhere close to VAM (Fig. 9(d)). Fig. 9(b) indicates that as a result of extreme underestimations in low-level warm moisture advection and convergence (which act as dynamic lifting mechanisms), mid-level vorticity was greatly underestimated, and was three orders of magnitude smaller than a typical dynamical definition of a mesocyclone.

(a) SA4.4 500 hPa relative vorticity and wind barbs at 15Z Run 11:00
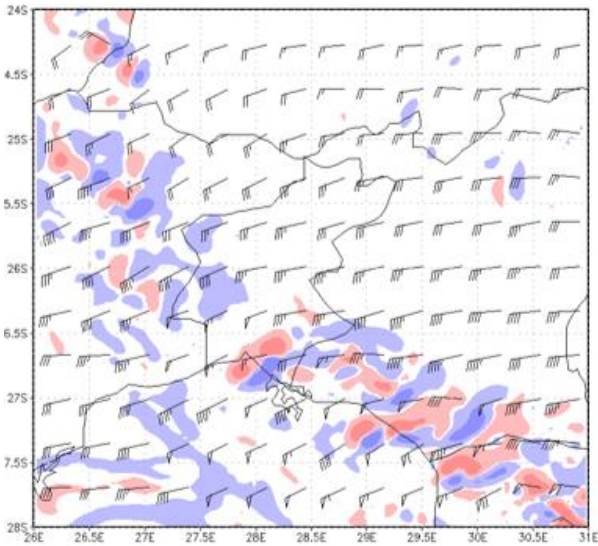
(b) SA1.5 500 hPa relative vorticity and wind barbs at 15Z Run 11:00
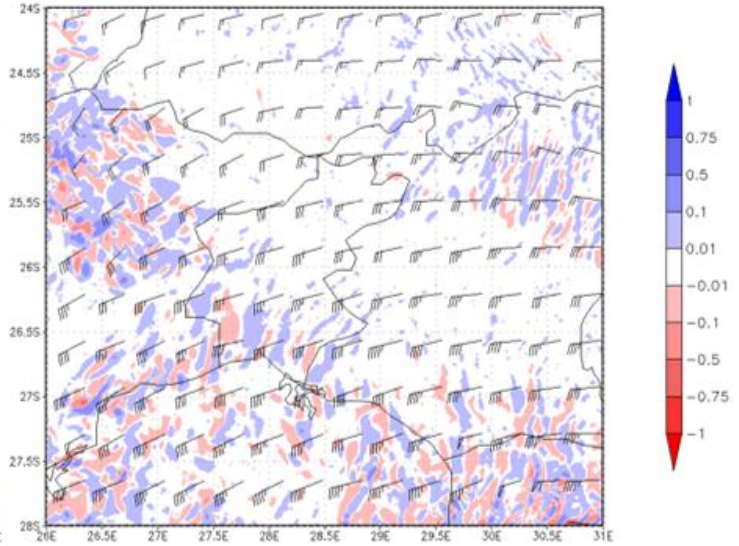
(c) SA4.4 800 hPa MFC and wind barbs at 15Z Run 11:00
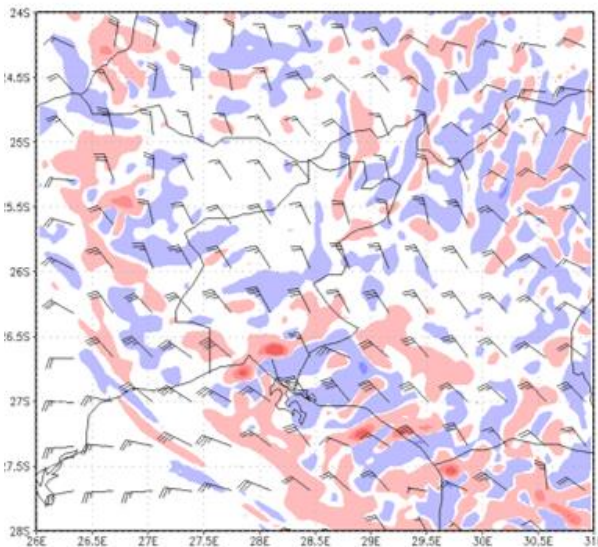
(d) SA1.5 800 hPa MFC and wind barbs at 15Z Run 11:00
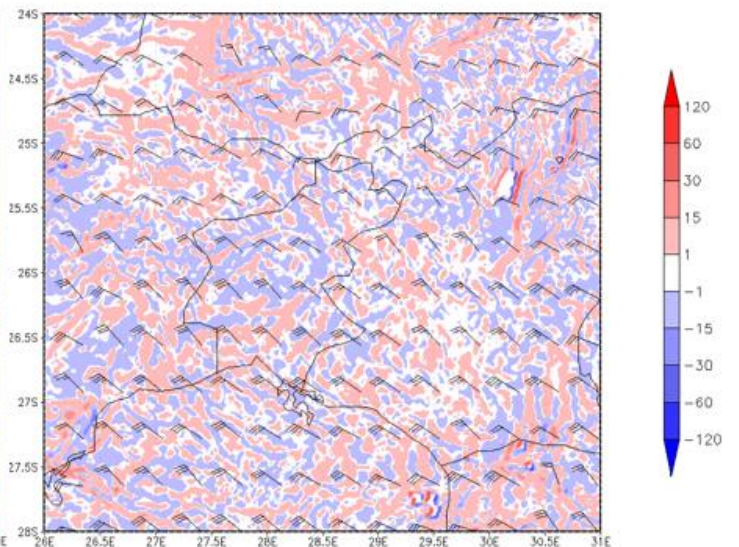
Figure 9: 500 hPa relative vorticity and wind barbs for (a) SA4.4 and (b) SA1.5. The shades in figures (a) and (b) represent negative (red) and positive (blue) relative vorticity in $10^{-2}\ s^{-1}$. MFC is in $10^{-6}\ g\ kg^{-1}s^{-1}$ and computed for (c) SA4.4 and (d) SA1.5 at 800 hPa with positive values (red shades) representing areas of convergence of moisture and negative values (blue) represents areas of divergence of moisture.

On the other hand, SA4.4 predicted a south-westerly propagation of 500 hPa vertical vorticity north of VAM between 15:00 UTC and 16:00 UTC (Fig. 9(a)). The maximum negative vorticity at 500 hPa reached by the VAM storm, as predicted

280   by SA4.4, ranged between -0.5×10^{-2} s^{-1} and -0.75×10^{-2} s^{-1} from 16:00 UTC and 17:00 UTC. This vertical vorticity was one order of magnitude smaller than a dynamical definition of a mesocyclone, which is an indicator that SA4.4 did not capture the mesocyclone of the VAM storm, and therefore underestimated its severity.

      A relationship between MFC and vertical vorticity was also determined. It was found that SA4.4 predicted vorticity maxima at 500 hPa that is associated with MFC maxima at 800 hPa. MFC initiates first at 800 hPa followed by vorticity

285   genesis at 500 hPa (Fig. 9(c)). This implies that the development of MFC in the low-levels could be a precursor of vertical vorticity initiation in the mid-levels. Since there is a positive relationship between low-level MFC and mid-level vorticity, it follows that the stronger the low-level MFC, the stronger the mid-level vorticity would be.

      Further examining the VAM storm during its 500 hPa vorticity maxima as predicted by SA4.4 (which occurred between 16:00 UTC and 17:00 UTC), reveals that low-level convergence occurred in the equatorward side of the storm, and

290   divergence in the polarward side of the storm. Figure 10(a) indicates that low-level convergence was associated with relatively higher values of specific humidity. This implies that there is an inflow of low-level moist air which converges in the equatorward side of the storm and then gets uplifted as updrafts. Figure 10(a) also indicates that low-level divergence is associated with relatively lower values of specific humidity which implies that there is low-level diverging dry-air in the polarward side of the storm. Figure 10(b) shows that the low-level diverging dry-air depicted in Figure 10(a) particularly

295   originates from the mid-levels.

(a) SA4.4 800 hPa convergence and specific humidity at 16Z Run 11:00
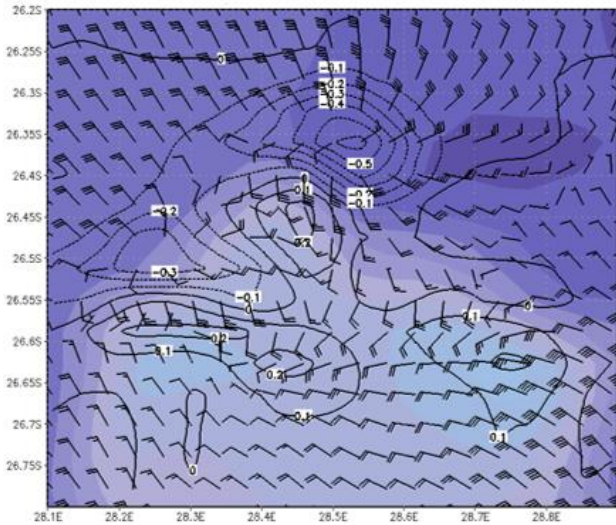
(b) SA4.4 500 hPa convergence and specific humidity at 16Z Run 11:00
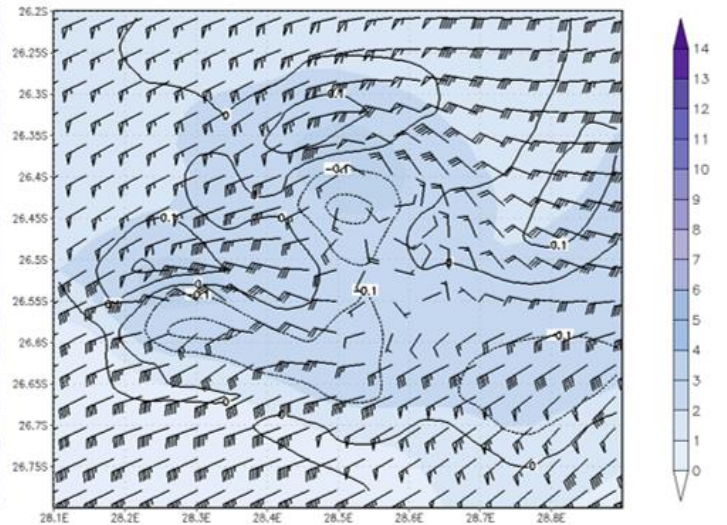
(c) SA4.4 10 m convergence and winds at 16Z Run 11:00
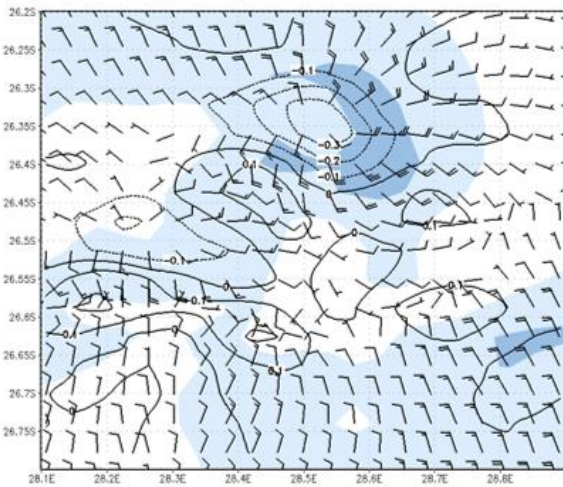
(d) SA4.4 500 hPa convergence and vorticity at 16Z Run 11:00
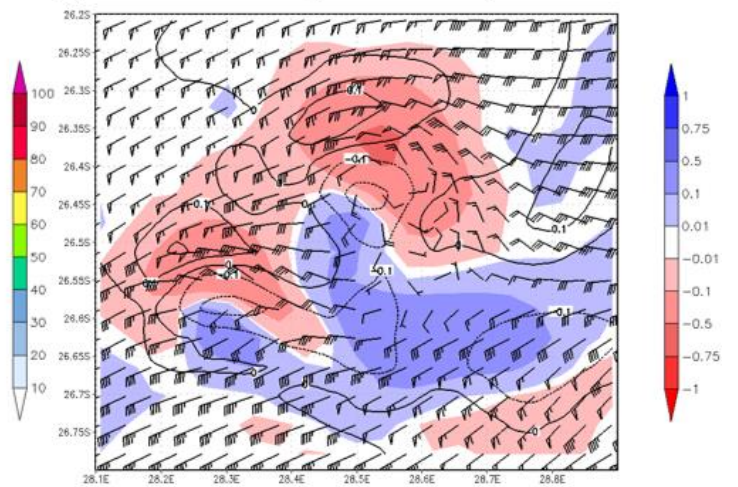
Figure 10: 16:00 UTC SA4.4 analysis of the (a) 800 hPa and (b) 500 hPa convergence/divergence (in $10^{-2}s^{-1}$) at contour intervals of $0.1 \times 10^{-2}s^{-1}$ and specific humidity (in $g\,kg^{-1}$) at shaded fields of interval $1 \times g\,kg^{-1}$. (c) Indicates 10 m convergence/divergence contour fields (in $10^{-2}s^{-1}$) at $0.1 \times 10^{-2}s^{-1}$ intervals and wind barbs and wind magnitude shades (in knots) at 10 knots intervals. (d) Indicates 500 hPa convergence/divergence (in $10^{-2}s^{-1}$) at contour intervals of $0.1 \times 10^{-2}s^{-1}$ and vorticity (in $10^{-2}s^{-1}$) shaded fields.

The analysis also indicates a coupling of 800 hPa convergence (divergence) fields with 500 hPa (divergence) convergence fields, which is an indicator that the low-level converging moist-air in the equatorward side of the storm gets uplifted with updrafts to the dry mid-levels then later gets advected to the low-levels with the downdrafts in the polarward side of the storm (Fig. 10(a) and 10(b)).

Figure 10(c) depicts 10 m winds and convergence (divergence) analysis. It should be noted that this analysis indicates that near-surface convergence (divergence) field patterns are similar to those at 800 hPa shown in Fig. 10(a), of which are together coupled with 500 hPa divergence (convergence) fields shown in Fig. 10(b). Figure 10(c) indicates that there are two

305   areas of updrafts origin near the surface (ahead of the storm and at the rear-flank of the storm) which are both located in the equatorward side of the storm, as also confirmed by the mid-level convergence and vorticity analysis (Fig. 10(d)). Figure 10(c) also indicates areas of forward-flank and rear-flank downdrafts which are in the polarward side of the storm as also confirmed by the mid-level convergence and vorticity analysis (Fig. 10(d)).

Figure 10 can be summarised as follows. There is a convergence of moist and relatively stronger surface and low-level

310   winds ahead of the storm which are uplifted as updrafts to the mid-levels. Some of these updrafts diverge as they reach the mid-levels and are later advected to the lower-levels and surface as relatively dry downdrafts, which then also diverge ahead of the downdraft area (toward the north-east as part of a front-flank gust front) and toward the rear-flank of the storm (toward the west as part of a rear-flank gust front) on reaching the surface. The north-eastward diverging winds then contribute to uplifting the inflowing moist air ahead of the storm. On the other hand, the westward diverging winds

315   converges with north-westerly inflowing moist-air in the rear-flank of the storm, initiating a second area of updrafts in the rear-flank of the storm. This rear-flank updrafts also diverge in the mid-levels and contribute to the forward-flank downdrafts. The diverging mid-level winds from the rear-flank updrafts also converge with mid-level dry-air which is being entrained from behind the storm and are later advected to the surface as the rear-flank downdrafts. This is significant, since as Davies-Jones et al. (2001) has shown, this rear-flank downdraft is important for tornadogenesis. Figure 10 further

320   indicates that surface and low-level convergence is associated with the storm's cyclonic updrafts, while divergence is associated with anticyclonic downdrafts.

It is interesting to note that this analysis indicates that SA4.4 predicted thunderstorm dynamics consisted with those of a classic supercell. Therefore, from a dynamical perspective, SA4.4 was able to predict the VAM supercell, even though its strength was underestimated, and location incorrect possibly due to a lack of data assimilation.

325   **3.4 Summary and conclusion**

In this study an analysis of the tornadic supercell that tracked through the northern parts of the Highveld in South Africa on 11 December 2017 was performed. It was found that this supercell initialised in the Free State Province as part of a cluster of multicellular thunderstorms over a dryline, and propagated in a north-easterly direction while strengthening and weakening throughout its lifetime, until it dissipated 7 hours later on approach to Machadodorp in the Mpumalanga Province. It was

330   also found that three ingredients were important in strengthening and maintaining this supercell: significant surface to mid-level vertical shear, an abundance of low-level warm moisture influx from the tropics and Mozambique Channel, and the relatively dry mid-levels.

On approach to the extreme south of the Gauteng Province, the already severe supercell encountered even more low-level moisture in the area which resulted in a tornado being initiated south of Deneysville town at approximately 17:15 local

335   time. The supercell tracked through the Vaal Dam, and continued through the town of Vaal Marina and the Mamello informal settlement at around 17:30 local time.

NWP models operationally run at the SAWS were also analysed and evaluated to see how they performed in predicting this tornadic supercell. It was found that the 4.4 km grid spacing model (SA4.4) performed better than the 1.5 km grid spacing model (SA1.5) in predicting this supercell. This is in spite of the horizontal resolution of SA1.5 being higher than that of SA4.4, and therefore, expected to be able to better represent small-scale atmospheric processes. The poor performance of SA1.5 seems to have emanated from a significant underestimation in low-level warm moisture advection and convergence (which act as dynamic lifting mechanisms), and as a result the mid-level vorticity being greatly underestimated, which led to the storm not being initialised.

SA4.4 was able to capture the supercell being analysed. However, the severity of this supercell was underestimated, possibly due to an underestimation in the mid-level vorticity which was found to be one order of magnitude smaller than that of a typical mesocyclone. This underestimation in mid-level vorticity was found to be a result of underestimated surface to mid-level vertical wind shear and underestimated low-level horizontal mass and moisture flux convergence. SA4.4 also predicted a correct timing of the supercell, however the location was incorrect possibly due to a lack of regional and local data assimilation.

From these results, it is recommended that research into the possibility and benefits of implementing dynamic and thermodynamic objective analysis schemes, which are derived from both NWP model data output and near real-time surface and upper-air observations, be conducted for a very short-range objective prediction of severe thunderstorm (including supercells) initiation over the central and eastern parts of South Africa.

Climate change is expected to result in frequent severe storms over southern Africa, therefore future investigations will involve experimental research over the Highveld region of South Africa to understand mesoscale and local dynamics processes responsible for tornadogenesis in some severe storms. Such a study, to the best of our knowledge, has never been conducted. This will help improve representation of regional and local processes in mesoscale NWP models which will in turn improve the skill of severe storm prediction over South Africa.

Data availability. The UM is licensed and legal possibilities of accessing its operational data should be cleared with the SAWS. Radiosonde data can be obtained from the Integrated Global Radiosonde Archive Version 2 (IGRA 2) via https://doi.org/10.7289/V5X63K0Q. Radar and weather stations data can be obtained from the SAWS. ERA5 data can be obtained from Copernicus Climate Change Service Climate Data Store via https://climate.copernicus.eu/climate-reanalysis.

Author contributions. LEL and MMB conceived and designed the study. LEL, GR, MMB and PM performed the analysis while continuously discussing results with all authors who in turn contributed through their feedback. GR, MG, LEL and NM curated the data. LEL wrote the initial draft of the manuscript with all authors reviewing and contributing in various

proportion to sections. All authors edited the final draft and provided significant comments and suggestions for further clarity and improvements.

Competing interests. The authors declare that they have no conflict of interest.

Acknowledgements. The authors thank the SAWS for providing model and observational data for this study. This work was partially supported through the Climate Research for Development (CR4D) Fellowship implemented by the African Academy of Sciences (AAS) in partnership with the United Kingdom's Department for International Development (DfID) Weather and Climate Information Services for Africa (WISER) programme and the African Climate Policy Centre (ACPC) of the United Nations Economic Commission for Africa (UNECA). The authors also acknowledge the SAWS for supporting this study.

375

References

Adger, W. N., Huq, S., Brown, K., Conway, D., and Hulme, M.: Adaptation to climate change in the developing world, Progress in Development Studies, 3, 179 – 195. doi: https://doi.org/10.1191/1464993403ps060oa, 2003.

Awojobi, O.N., and Tetteh, J.: The impacts of climate change in Africa: A review of the scientific literature, Journal of International Academic Research for Multidisciplinary, 5, 39 – 52, 2017.

Banacos, P.C., and Schultz, D.M.: The use of moisture flux convergence in forecasting convective initiation: Historical and operational perspectives, Wea. Forecasting, 20, 351 – 366. doi: https://doi.org/10.1175/WAF858.1, 2005.

Boko, M., Niang, I., Nyong, A., Vogel, C., Githeko, A., Medany, M., Osman-Elasha, B., Tabo, R. and Yanda, P.: Africa. Climate Change 2007: Impacts, Adaptation and Vulnerability. Contribution of Working Group II to the Fourth Assessment Report of the Intergovernmental Panel on Climate Change, M.L. Parry, O.F. Canziani, J.P. Palutikof, P.J. van der Linden and C.E. Hanson, Eds., Cambridge University Press, Cambridge UK, 433-467, 2007.

Craven J. P., and Brooks, H.E.: Baseline climatology of sounding-derived parameters associated with deep moist convection, National Weather Digest, 28, 13–24, 2004.

Dahl, J.M.L.: Tilting of horizontal shear vorticity and the development of updraft rotation in supercell thunderstorms, Journal of the Atmospheric Sciences, 74, 2997-3020. doi: https://doi.org/10.1175/JAS-D-17-0091.1, 2017.

Davies, T., Cullen, M.J.P., Malcolm, A.J., Mawson, M.H., Staniforth, A., White, A.A., and Wood, N.: A new dynamical core for the Met Office's global and regional modeling of the atmosphere, Quarterly Journal of the Royal Meteorological Society, 131, 1759–1782. doi: https://doi.org/10.1256/qj.04.101, 2005.

Davies-Jones, R., Trapp, R.J., and Bluestein, H.B.: Tornadoes and tornadic storms (chapter 5), Meteorological Monographs, 28, 167 – 221. doi: https://doi.org/10.1007/978-1-935704-06-5_5, 2001.

Davies-Jones, R.: A review of supercell and tornado dynamics, Atmospheric Research, 158, 274 – 291. DOI: https://doi.org/10.1016/j.atmosres.2014.04.007, 2015.

Davis-Reddy, C.L., and Vincent, K.: Climate risk and vulnerability: A handbook for southern Africa, 2nd ed., CSIR, Pretoria, South Africa, 2017.

DEA: Long-Term Adaptation Scenarios Flagship Research Programme for South Africa: Summary for Policy-Makers, Department of Environmental Affairs, Pretoria, South Africa, 2016.

Doswell, C.A., and Burgess, D.W.: On some issues of United States tornado climatology, Monthly Weather Review, 116, 495-501. doi: https://doi.org/10.1175/1520-0493(1988)116%3C0495:OSIOUS%3E2.0.CO;2, 1988.

EASAC: Extreme weather events in Europe: Preparing for climate change adaptation: an update on EASAC's 2013 study, EASAC, Teutschenthal, Germany, pp. 1 – 8, 2018.

Engelbrecht, C.J., Engelbrecht, F.A., and Dyson, L.L.: High-resolution model-projected changes in mid-tropospheric closed-lows and extreme rainfall events over southern Africa, Int. J. Climatol., 33, 173 – 187. doi: https://doi.org/10.1002/joc.3420, 2013.

Gijben, M.: The lightning climatology of South Africa, South African Journal of Science, 108, 1-10. doi: https://doi.org/10.4102/sajs.v108i3/4.740, 2012.

Glickman, T.S. (Ed.): Glossary of Meteorology, 2nd ed., American Meteorological Society, Boston, 2000.

Goliger, A.M., and Retief, J.V.: Severe wind phenomena in Southern Africa and the related damage, Journal of Wind Engineering and Industrial Aerodynamics, 95, 1065-1078. doi: https://doi.org/10.1016/j.jweia.2007.01.029, 2007.

Hamill, T.M., Schneider, R.S., Brooks, H.E., Forbes, G.S., Bluestein, H.B., Steinberg, M., Melendez, D., and Dole, R.M.: The May 2003 extended tornado outbreak, Bulletin of the American Meteorological Society, 86, 531 – 542. doi: https://doi.org/10.1175/BAMS-86-4-531, , 2005.

Handmer, J., Honda, Y., Kundzewicz, Z.W., Arnell, N., Benito, G., Hatfield, J., Mohamed, I.F., Peduzzi, P., Wu, S., Sherstyukov, B., Takahashi, K., and Yan, Z.: Changes in impacts of climate extremes: human systems and ecosystems. In: Managing the Risks of Extreme Events and Disasters to Advance Climate Change Adaptation [Field, C.B., V. Barros, T.F. Stocker, D. Qin, D.J. Dokken, K.L. Ebi, M.D. Mastrandrea, K.J. Mach, G.-K. Plattner, S.K. Allen, M. Tignor, and P.M. Midgley (eds.)], A Special Report of Working Groups I and II of the Intergovernmental Panel on Climate Change (IPCC), Cambridge University Press, Cambridge, UK, and New York, NY, USA, pp. 231-290, 2012.

Hart, N.C.G., Reason, C.J.C., and Fauchereau, N.: Cloud bands over southern Africa: seasonality, contribution to rainfall variability and modulation by the MJO, Clim. Dyn., 41, 1199 – 1212. doi: https://doi.org/10.1007/s00382-012-1589-4, 2013.

Helmus, J.J., and Collis, S.M.: The Python ARM Radar Toolkit (Py-ART), a Library for Working with Weather Radar Data in the Python Programming Language. Journal of Open Research Software, 4, p.e25. doi: http://doi.org/10.5334/jors.119, 2016.

Hersbach, H., and Dee, D.: ERA5 reanalysis is in production. ECMWF Newsletter. Vol. 147, p. 7. Available at:
430   https://www.ecmwf.int/en/newsletter/147/news/era5-reanalysis-production (Accessed: 14 February 2019), 2016.

Holton, J.R., and Hakim, G.J.: An Introduction to Dynamic Meteorology, 5th ed., Academic Press, San Diego. doi: https://doi.org/10.1016/B978-0-12-384866-6.00001-5, 2013.

Houze, R.A.: Cloud Dynamics, Academic Press, San Diego, 1993.

IPCC: Climate Change 2014: Impacts, Adaptation, and Vulnerability. Part A: Global and Sectoral Aspects. Contribution of
435   Working Group II to the Fifth Assessment Report of the Intergovernmental Panel on Climate Change [Field, C.B., V.R. Barros, D.J. Dokken, K.J. Mach, M.D. Mastrandrea, T.E. Bilir, M. Chatterjee, K.L. Ebi, Y.O. Estrada, R.C. Genova, B. Girma, E.S. Kissel, A.N. Levy, S. MacCracken, P.R. Mastrandrea, and L.L.White (eds.)], Cambridge University Press, Cambridge, United Kingdom and New York, NY, USA, 1132 pp, 2014.

Kruger, A.C., and Nxumalo, M.P.: Historical rainfall trends in South Africa: 1921–2015, Water SA, 43 (2), 285 – 297. doi:
440   https://doi.org/10.4314/wsa.v43i2.12, 2017.

Malherbe, J., Engelbrecht, F.A., and Landman, W.A.: Projected changes in tropical cyclone climatology and landfall in the Southwest Indian Ocean region under enhanced anthropogenic forcing, Clim, Dyn., 40, 2867 – 2886. doi: https://doi.org/10.1007/s00382-012-1635-2, 2013.

Markowski, P.M., and Richardson, Y.P.: Tornadogenesis: Our current understanding, forecasting considerations, and
445   questions to guide future research, Atmospheric Research, 93, 3-10. doi: https://doi.org/10.1016/j.atmosres.2008.09.015, 2009

Mashaba, S., and ANA reporter: WATCH: Night of horror as tornado hits Vaal Marina, IOL, 13 December 2017. Available at: https://www.iol.co.za/news/south-africa/gauteng/watch-night-of-horror-as-tornado-hits-vaal-marina-12392994 (Accessed: 21 August 2018) , 2017.

450   Meehl, G.A., Karl, T., Easterling, D.R., Changnon, S., Pielke Jr., R., Changnon, D., Evans, J., Groisman, P., Knutson, T.R., Kunkel, K.E., Mearns, L.O., Parmesan, C., Pulwarty, R., Root, T., Sylves, R.T., Whetton, P., and Zwiers, F.: An introduction to trends in extreme weather and climate events: Observations, socioeconomic impacts, terrestrial ecological impacts, and model projections, Bull. Amer. Meteor. Soc., 81, 413 – 416. doi: https://doi.org/10.1175/1520-0477(2000)081%3C0413:AITTIE%3E2.3.CO;2, 2000.

455   Melillo, J.M., Richmond, T.C., and Yohe, G.W., Eds.: Climate Change Impacts in the United States: The Third National Climate Assessment. U.S. Global Change Research Program. 841 pp. doi: https://doi.org/10.7930/J0Z31WJ2, 2014.

Mirza, M.M.Q.: Climate change and extreme weather events: can developing countries adapt?, Clim. Policy, 3, 233 – 248. doi:10.1016/S1469-3062(03)00052-4, 2003.

Mitchley, A.: PICS: Over 30 injured, 300 homes damaged as tornado tears through Vaal Marina, News24, 12 December
460   2017. Available at: https://www.news24.com/SouthAfrica/News/pics-over-30-injured-300-homes-damaged-as-tornado-tears-through-vaal-marina-20171212 (Accessed: 21 August 2018) , 2017.

NDMC: Annual Report 2017/2018, National Disaster Management Centre, Pretoria, South Africa, 2018.

Nuttall, M.: Protecting the Arctic: Indigenous Peoples and Cultural Survival, Routledge, London, 195 pp, 1998.

Rae, K.J.: A modified Supercell Composite Parameter for supercell thunderstorms over the Gauteng Province, South Africa,
465   Masters Dissertation, University of Pretoria, South Africa, 2014.

Reason, C.J.C., and Keibel, A.: Tropical cyclone Eline and its unusual penetration and impacts over the Southern African
        mainlands, Wea. Forecasting, 19, 789 – 805. doi: https://doi.org/10.1175/1520-0434(2004)019%3C0789:TCEAIU%3E2.0.CO;2, 2004 .

SABC: Midvaal residents affected by tornado to be housed at churches and community centres, SABC, 12 December 2017.
470   Available at: https://www.youtube.com/watch?v=dXcPFF1lTIg (Accessed: 21 August 2018) , 2017.

SAWS: Climate Summary of South Africa, South African Weather Service, 28 (12), 1 - 5, 2018.

Storm Report SA: Photos taken by Celestine Lourens of the tornado and damage in Vaal Marina today!, Storm Report SA,
        11 December 2017. Available at: https://www.facebook.com/stormreportsaOFFICIAL/posts/1603665363029458 (Accessed: 21 August 2018) , 2017.

475 Tyson, P. D., and Preston-Whyte, R. A.: The Weather and Climate of Southern Africa, 2nd ed., Oxford University Press, 396
        pp, 2000.

UN: The Least Developed Countries Report 2018, United Nations Publications, New York, 159 pp, 2018a.

UN: World Economic Situation and Prospects 2018, United Nations Publication, New York, 187 pp, 2018b.

Walters, D., Boutle, I., Brooks, M., Melvin, T., Stratton, R., Vosper, S., Wells, H., Williams, K., Wood, N., Allen, T.,
480   Bushell, A., Copsey, D., Earnshaw, P., Edwards, J., Gross, M., Hardiman, S., Harris, C., Heming, J., Klingaman, N.,
        Levine, R., Manners, J., Martin, G., Milton, S., Mittermaier, M., Morcrette, C., Riddick, T., Roberts, M., Sanchez, C.,
        Selwood, P., Stirling, A., Smith, C., Suri, D., Tennant, W., Vidale, P.L., Wilkinson, J., Willett, M., Woolnough, S., and
        Xavier, P.: The Met Office Unified Model Global Atmosphere 6.0/6.1 and JULES Global Land 6.0/6.1 configurations,
        Geosci. Model Dev., 10, 1487–1520. doi: https://doi.org/10.5194/gmd-10-1487-2017, 2017.

485 WMO: Reducing Vulnerability to Extreme Hydro-Meteorological Hazards in Mozambique After Cyclone IDAI, World
        Meteorological Organisation, Geneva, 64 pp. Available at: https://library.wmo.int/doc_num.php?explnum_id=6259 (Accessed: 21 July 2020) , 2019.

Wood, N., Staniforth, A., White, A., Allen, T., Diamantakis, M., Gross, M., Melvin, T., Smith, C., Vosper, S., Zerroukat, M.,
        and Thuburn, J.: An inherently mass-conserving semi-implicit semi-Lagrangian discretization of the deep-atmosphere
490   global non-hydrostatic equations, Q. J. Roy. Meteorol. Soc., 140, 1505– 1520. doi: https://doi.org/10.1002/qj.2235,
        2014.